Modeling and μ Synthesis Control of Vehicle Active Suspension with Motor Actuator

YONGCHAO ZHANG, GUOGUANG ZHANG, FAN YU*
State Key Laboratory Mechanical System & Vibration, School of Mechanical Engineering
Shanghai Jiao Tong University
800 Dongchuan RD. Minhang District, Shanghai
CHINA
fanyu@sjtu.edu.cn

Abstract: This paper presents the modeling and μ synthesis for a vehicle active suspension system with a motor actuator, and analyses the performances of the active suspension with μ synthesis controller. Firstly, considering parameter uncertainties and unmodeled dynamics of suspension and motor actuator, an uncertain model has been built by linear fraction transformation. Secondly, a μ synthesis controller is designed for this uncertain system. Finally, frequency and time responses of passive and active suspensions have been obtained by simulation. For comparison purpose, an H_∞ synthesis controller is proposed as well. The results show that the designed μ synthesis controller can improve ride comfort significantly compared with passive suspension, and is slightly worse than the H_∞ synthesis controller in the sensitive frequency range for human. Both robust stability and robust performance of the perturbed system with the μ synthesis controller have been verified by μ analysis method, indicating significantly superiority to the H_∞ synthesis controller. Additionally, the sensitiveness of uncertainties is demonstrated by illustrations of perturbed systems with parameter variations.

Key-Words: Active Vehicle Suspension, Motor Actuator, μ Synthesis, Robust Stability, Robust Performance

1 Introduction

The aims of vehicle active suspension are to improve ride comfort by suppressing the vibrations from road roughness and provide good handling performance. Since random road excitation is actually a disturbance with limited energy band, the active suspension is designed to attenuate the road disturbance and achieve a trade-off between the conflicting suspension performance requirements. Additionally, the uncertainties of actual suspension system usually including parameter variations of suspension and unmodeled dynamics of actuator affect the suspension performances and even result in the instability of suspension system.

Several controllers have been proposed to solve these problems of active suspension. The linear quadratic Gaussion (LQG) controller can attenuate road disturbance and measurement noise effectively [1-3], but it has a poor stability margin for uncertain system, i.e., system may be unstable in the presence of the uncertainties. Then, H_∞ synthesis is used to deal with the uncertainties in an unstructured way and provides an optimal controller to ensure the robustness and required performances of suspension system [4-9]. In spite of this, the controller is too conservative [10]. In addition, another useful strategy, i.e., linear parameter varying (LPV) control combining H_∞ synthesis with gain-scheduling approach [11-14], is applied to active suspension. LPV controller is gain-scheduled by the measured or estimated information of variable parameters to adapt to the variation of parameters. But it cannot deal with unmodeled dynamics of actuator. In a word, the above three controllers are undesirable for the perturbed system with the mixed uncertainties including parameter variations and unmodeled dynamics.

In order to concern the mixed uncertainties and reduce the conservativeness of controller, the mixed μ synthesis controller is designed for active suspension [15, 16]. In the design process, μ synthesis controller applies the structured uncertainties, providing more detailed information of uncertainty characteristics, so that it can ensure robust stability and robust performance of the perturbed system.

In this study, the research work is carried out on the developed suspension system which is featured by a type of DC motor actuator produced by SJTU [17-19]. Due to the special structure of ball screw-nut mechanism, the moments of inertia of rotor and nut can affect directly the performances of controlled suspension. Meanwhile, the unmodeled high-order dynamics of the motor's control circuit

will also influence the system robustness significantly. Therefore, these two elements should be considered in the actuator model. In addition, the practical suspension system always varies with operation conditions. For instance, the sprung mass varies in a large range with the number of passengers, which may degrade the suspension performances. Other variable parameters, such as the stiffness of suspension spring and tire, the damping of actuator and motor constant, are also important to ensure the effectiveness of the control. Hence, the multiple parameter uncertainties should be taken into account in the suspension model.

Based on the literature review of control strategies for vehicle active suspensions and the uncertain model with the mixed uncertainties including parameter uncertainties and unmodel dynamics, μ synthesis method is adopted to design the controller for the active suspension with motor actuator.

In general, this paper focuses on the modeling of a vehicle active suspension system with a DC motor actuator and proposes a robust control with μ synthesis method to deal with the mixed uncertainties. For comparison purpose, an H_∞ synthesis controller is also designed.

The structure of the paper is as follows. Section 2 presents the modeling of suspension system. Section 3 discusses the robust control design based on μ synthesis and H_∞ synthesis. And Section 4 shows the benefits of μ synthesis controller through performance comparison with passive suspension and H_∞ synthesis controller.

2 MODELING OF SUSPENSION AND MOTOR SYSTEM

2.1 Quarter-vehicle Suspension Model

The suspension model usually includes quarter-vehicle model, half vehicle model and full vehicle model [20]. Although the quarter-vehicle model with two degrees of freedom (2DOF) [1] is simple, it is effective to have a good understanding of suspension performances, such as ride comfort and road holding. The half vehicle model (4DOF) is used to evaluate pitch and bounce of vehicle body, especially with wheelbase preview control [2], while the full vehicle model (7DOF) [4] is more complicated and accurate to evaluate the attitude of vehicle body, i.e., pitch, roll and bounce. The results of the controllers for the quarter-vehicle model always coincide with that of the half/full vehicle models to a great extent, although it is accepted that further important practical problems appear when the control strategy is implemented on the half/full vehicle models. Hence, the quarter-vehicle suspension model is used as shown in Fig.1. C_f represents the equivalent damper coefficient of motor actuator. The active force F_o is provided by motor actuator. The dynamic equations of the suspension system are as follows:

$$m_b\ddot{x}_b = -K_s(x_b - x_w) - C_f(\dot{x}_b - \dot{x}_w) + F_o \quad (1)$$

$$m_w\ddot{x}_w = K_s(x_b - x_w) + C_f(\dot{x}_b - \dot{x}_w) - K_t(x_w - x_g) - F_o \quad (2)$$

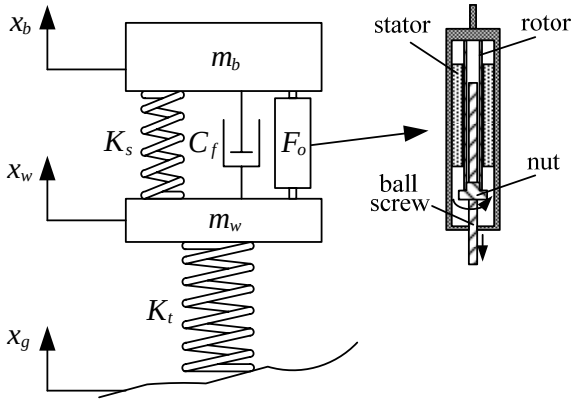

Fig.1 Quarter-vehicle suspension model

2.2 Motor Dynamic Model

The developed prototype of motor actuator is composed of a three-phase permanent-magnet brushless DC motor, a ball screw and a nut, as shown in Fig.2. The rotor angular motion is converted to the ball screw linear motion by the nut. Thus, the motor output torque can be transferred to the active vertical force. Due to the high rotor speed during the suspension operation, the high frequency effects of the moment of inertia of rotor and nut should be considered. The dynamic model for the rotor and the nut is demonstrated in Fig.3.

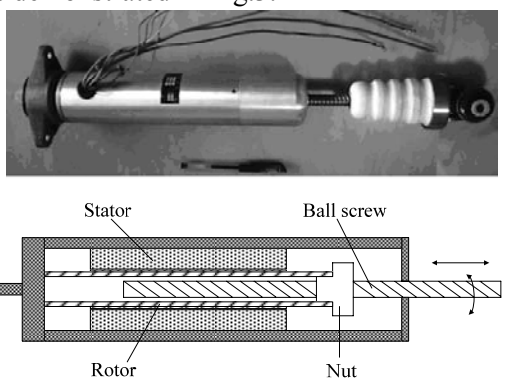

Fig.2 Prototype and schematic diagram of motor actuator

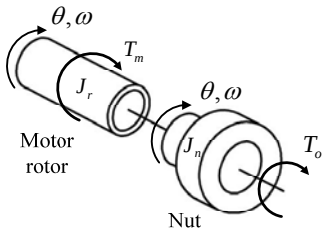

Fig.3 Dynamic model for rotor and nut

According to the transformation of ball screw, the equation can be written as below:

$$\omega = \frac{2\pi v_s}{P_l} \tag{3}$$

where ω is angular velocity, $v_s = \dot{x}_b - \dot{x}_w$ is suspension stroke velocity and P_l is the lead of ball screw. The dynamic model can be expressed by the following equation:

$$(J_r + J_n)\dot{\omega} = T_m - T_o \tag{4}$$

where T_m is motor output torque and T_o is actual total output torque, and J_n and J_r are moments of inertia of nut and motor rotor, respectively. The motor output torque can be calculated from motor control current i, i.e.,

$$T_m = K_T i \tag{5}$$

in which K_T is torque constant of motor. Then, the output force F_o from ball screw can be obtained as

$$F_o = \frac{2\pi T_o}{P_l} \tag{6}$$

From equations (3)~(6), the output force of motor actuator can be expressed as

$$F_o = \Phi i - I_d \dot{v}_s \tag{7}$$

where $\Phi = \frac{2\pi K_T}{P_l}$, $I_d = \frac{4\pi^2 (J_r + J_n)}{P_l^2}$.

From (1), (2) and (7), the dynamic equations of suspension model are as follows:

$$\begin{aligned}\ddot{x}_b = \frac{1}{m_b(m_w + I_d) + m_w I_d}\Big[&-m_w K_s (x_b - x_w) \\ &-m_w C_f (\dot{x}_b - \dot{x}_w) + m_w \Phi i - I_d K_t (x_w - x_g)\Big]\end{aligned} \tag{8}$$

$$\begin{aligned}\ddot{x}_w = {}&\gamma_1\Big[K_s (x_b - x_w) + C_f (\dot{x}_b - \dot{x}_w) - \Phi i - K_t (x_w - x_g)\Big] \\ &+ \frac{1}{m_b(m_w + I_d) + m_w I_d}\Big\{-\gamma_1\gamma_2\Big[K_s (x_b - x_w) \\ &+ C_f (\dot{x}_b - \dot{x}_w) - \Phi i\Big] + (\gamma_1\gamma_2 - I_d) K_t (x_w - x_g)\Big\}\end{aligned} \tag{9}$$

where $\gamma_1 = \frac{1}{m_w + I_d}$, $\gamma_2 = m_w I_d$.

Since body mass varies from empty-load to full-load within a wide range, it is a significant uncertain parameter for suspension characteristics. Because of the non-linearity of suspension spring and actuator friction, the variations of spring stiffness and damping coefficient also need to be considered. Due to the change of temperature and pressure, tire stiffness is assumed to be uncertain. In addition, the non-linearity of motor model cannot be neglected, e.g. the motor constant may be inaccurate as a result of the measurement error, etc. Hence, five main uncertain parameters are selected in a range of practical variations around their nominal values, respectively,

$$\begin{aligned} m_b &= \bar{m}_b (1 + d_{mb}\delta_{mb}) \\ K_s &= \bar{K}_s (1 + d_{ks}\delta_{ks}) \\ K_t &= \bar{K}_t (1 + d_{kt}\delta_{kt}) \\ C_f &= \bar{C}_f (1 + d_{cf}\delta_{cf}) \\ \Phi &= \bar{\Phi}(1 + d_{\Phi}\delta_{\Phi}) \end{aligned}$$

where $d_{mb} = 0.2$, $d_{ks} = 0.2$, $d_{kt} = 0.1$, $d_{cf} = 0.2$, $d_{\Phi} = 0.2$, $\|\delta_{mb}\|, \|\delta_{ks}\|, \|\delta_{kt}\|, \|\delta_{cf}\|, \|\delta_{\Phi}\| \le 1$. The scalars, denoted as d, represent the percentages of variation around the nominal values and indicate the degree of parameter uncertainty. And $\|\delta\|$ represents the norm of the actual parameter deviation. The symbols m_b, K_s, K_t, C_f, Φ, respectively refer to the above 5 uncertain parameters and $\bar{m}_b, \bar{K}_s, \bar{K}_t, \bar{C}_f, \bar{\Phi}$ are defined as corresponding nominal parameters.

All uncertainty parameters can be written in the form of lower Linear Fractional Transformation (LFT), which is necessary for structure uncertainty analysis. The LFT representations are expressed as follows:

$$\begin{aligned}&\frac{1}{m_b(m_w + I_d) + m_w I_d} \\ &= \beta + (-\alpha)\delta_{mb}\left[1 - (-\alpha)\delta_{mb}\right]^{-1}\beta \\ &= F_l\left(\begin{bmatrix}\beta & -\alpha \\ \beta & -\alpha\end{bmatrix}, \delta_{mb}\right) = F_l(M_{mb}, \delta_{mb})\end{aligned} \tag{10}$$

$$\begin{aligned}K_s &= \bar{K}_s (1 + d_{ks}\delta_{ks}) \\ &= F_l\left(\begin{bmatrix}\bar{K}_s & d_{ks} \\ \bar{K}_s & 0\end{bmatrix}, \delta_{ks}\right) = F_l(M_{ks}, \delta_{ks})\end{aligned} \tag{11}$$

$$\begin{aligned}K_t &= \bar{K}_t (1 + d_{kt}\delta_{kt}) \\ &= F_l\left(\begin{bmatrix}\bar{K}_t & d_{kt} \\ \bar{K}_t & 0\end{bmatrix}, \delta_{kt}\right) = F_l(M_{kt}, \delta_{kt})\end{aligned} \tag{12}$$

$$C_f = \bar{C}_f\left(1+d_{cf}\delta_{cf}\right) = F_l\left(\begin{bmatrix}\bar{C}_f & d_{cf}\\ \bar{C}_f & 0\end{bmatrix},\delta_{cf}\right) = F_l\left(M_{cf},\delta_{cf}\right) \tag{13}$$

$$\Phi = \bar{\Phi}(1+d_\Phi\delta_\Phi) = F_l\left(\begin{bmatrix}\bar{\Phi} & d_\Phi\\ \bar{\Phi} & 0\end{bmatrix},\delta_\Phi\right) = F_l\left(M_\Phi,\delta_\Phi\right) \tag{14}$$

in which $\alpha = \dfrac{\bar{m}_b d_{mb}}{\bar{m}_b+\gamma_1\gamma_2}$, $\beta = \dfrac{\gamma_1}{\bar{m}_b+\gamma_1\gamma_2}$.

$\delta_j\left(j\in\left(mb,ks,kt,cf,\Phi\right)\right)$ represents the uncertainty which can be extracted from the differential equations by the LFT representation. Define that $p=\left[p_{mb1}\ p_{mb2}\ p_{ks}\ p_{kt}\ p_{cf}\ p_\Phi\right]^T$ and $q=\left[q_{mb1}\ q_{mb2}\ q_{ks}\ q_{kt}\ q_{cf}\ q_\Phi\right]^T$ are the inputs and outputs of δ_j blocks, respectively.

According to equations (8)~(14), the system block diagram with uncertain parameters can be obtained in Fig.4.

Three necessary suspension performances are chosen, i.e. body acceleration (BA), suspension working space (SWS) and dynamic tire deflection (DTD), as the performance outputs $z_p=\left[z_1\ z_2\ z_3\right]^T=\left[\text{BA SWS DTD}\right]^T$. The measured outputs are obtained by two linear potentiometers, whose voltages are given by $y=\left[y_1\ y_2\right]^T=\left[\text{BA}_\text{m}\ \text{SWS}_\text{m}\right]^T$. α_1 and α_2 are the gains of accelerometer and displacement meter, respectively. By defining the state vector and input vector respectively as $X=\left[x_b\ \dot{x}_b\ x_w\ \dot{x}_w\right]^T$ and $u_1=\left[x_g\ n\ i\right]^T$, where $n=\left[n_1\ \ n_2\right]^T$ are two noises of y, respectively, the corresponding differential equations of the above uncertain model can be expressed as below:

$$\begin{aligned}\ddot{x}_b = &-\beta m_w\bar{K}_s\left(x_b-x_w\right)-\beta m_w\bar{C}_f\left(\dot{x}_b-\dot{x}_w\right)\\ &+\beta m_w\bar{\Phi}i-\beta I_d\bar{K}_t\left(x_w-x_g\right)-\alpha p_{mb1}\\ &-\beta m_w d_{ks}p_{ks}-\beta I_d d_{kt}p_{kt}-\beta m_w d_{cf}p_{cf}\\ &+\beta m_w d_\Phi p_\Phi\end{aligned} \tag{15}$$

$$\begin{aligned}\ddot{x}_w = &\left(\gamma_1-\beta\gamma_1\gamma_2\right)\left[\bar{K}_s\left(x_b-x_w\right)+\bar{C}_f\left(\dot{x}_b-\dot{x}_w\right)\right.\\ &\left.-\bar{\Phi}i\right]+\left(-\gamma_1+\beta\gamma_1\gamma_2-\beta I_d\right)\bar{K}_t\left(x_w-x_g\right)\\ &-\alpha p_{mb2}+\left(\gamma_1-\beta\gamma_1\gamma_2\right)d_{ks}p_{ks}\\ &+\left(-\gamma_1+\beta\gamma_1\gamma_2-\beta I_d\right)d_{kt}p_{kt}\\ &+\left(\gamma_1-\beta\gamma_1\gamma_2\right)d_{cf}p_{cf}\\ &+\left(-\gamma_1+\beta\gamma_1\gamma_2\right)d_\Phi p_\Phi\end{aligned} \tag{16}$$

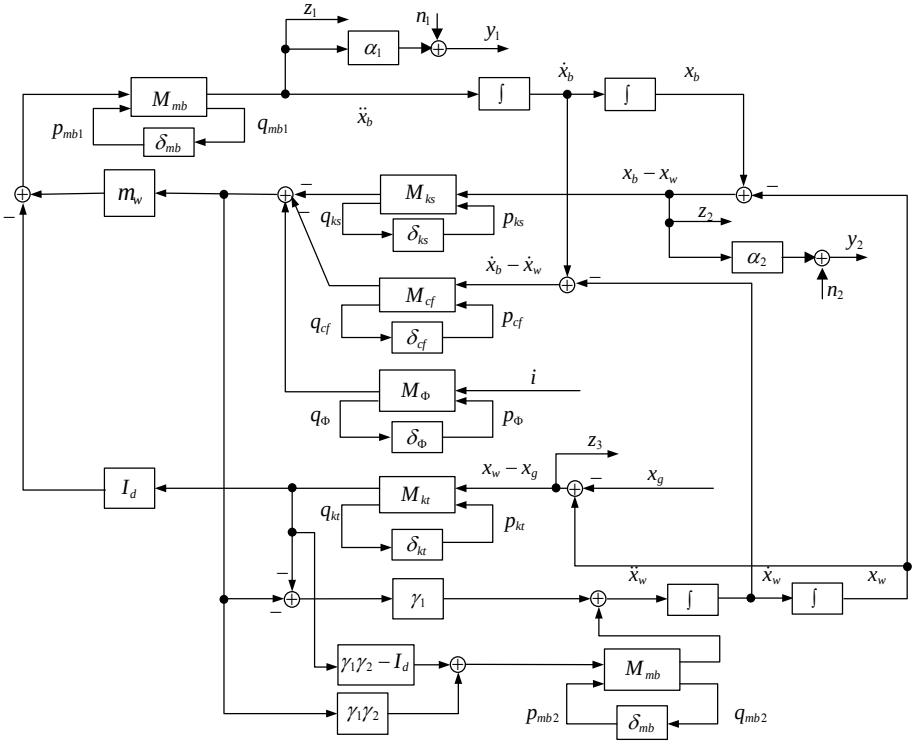

Fig.4 Control block diagram of suspension system

$$\begin{aligned} q_{mb1} &= -\beta m_w \bar{K}_s \left(x_b - x_w\right) - \beta m_w \bar{C}_f \left(\dot{x}_b - \dot{x}_w\right) \\ &\quad + \beta m_w \bar{\Phi} i - \beta I_d \bar{K}_t \left(x_w - x_g\right) - \alpha p_{mb1} \\ &\quad - \beta m_w d_{ks} p_{ks} - \beta I_d d_{kt} p_{kt} - \beta m_w d_{cf} p_{cf} \\ &\quad + \beta m_w d_\Phi p_\Phi \end{aligned} \tag{17}$$

$$\begin{aligned} q_{mb2} &= -\beta\gamma_1\gamma_2 \left[\bar{K}_s \left(x_b - x_w\right) + \bar{C}_f \left(\dot{x}_b - \dot{x}_w\right)\right. \\ &\quad \left. - \bar{\Phi} i\right] + \beta\left(\gamma_1\gamma_2 - I_d\right)\bar{K}_t \left(x_w - x_g\right) - \alpha p_{mb2} \\ &\quad - \beta\gamma_1\gamma_2 d_{ks} p_{ks} + \beta\left(\gamma_1\gamma_2 - I_d\right) d_{kt} p_{kt} \\ &\quad - \beta\gamma_1\gamma_2 d_{cf} p_{cf} + \beta\gamma_1\gamma_2 d_\Phi p_\Phi \end{aligned} \tag{18}$$

$$q_{ks} = \bar{K}_s \left(x_b - x_w\right) \tag{19}$$

$$q_{kt} = \bar{K}_t \left(x_w - x_g\right) \tag{20}$$

$$q_{cf} = \bar{C}_f \left(\dot{x}_b - \dot{x}_w\right) \tag{21}$$

$$q_\Phi = \bar{\Phi} i \tag{22}$$

$$\begin{aligned} z_1 = \ddot{x}_b &= -\beta m_w \bar{K}_s \left(x_b - x_w\right) - \beta m_w \bar{C}_f \left(\dot{x}_b - \dot{x}_w\right) \\ &\quad + \beta m_w \bar{\Phi} i - \beta I_d \bar{K}_t \left(x_w - x_g\right) - \alpha p_{mb1} \\ &\quad - \beta m_w d_{ks} p_{ks} - \beta I_d d_{kt} p_{kt} - \beta m_w d_{cf} p_{cf} \\ &\quad + \beta m_w d_\Phi p_\Phi \end{aligned} \tag{23}$$

$$z_2 = x_b - x_w \tag{24}$$

$$z_3 = x_w - x_g \tag{25}$$

$$y_1 = \alpha_1 \ddot{x}_b \tag{26}$$

$$y_2 = \alpha_2 \left(x_b - x_w\right) \tag{27}$$

Thus, the perturbed suspension model with measurement noises is summarized as

$$\begin{bmatrix} \dot{X} \\ \hline q \\ \hline z_p \\ \hline y \end{bmatrix} = \left[\begin{array}{c|c|c|c} A & B_p & B_1 & B_2 \\ \hline C_q & D_{qp} & D_{q1} & D_{q2} \\ \hline C_z & D_{zp} & D_{z1} & D_{z2} \\ \hline C_y & D_{yp} & D_{y1} & D_{y2} \end{array}\right] \begin{bmatrix} X \\ \hline p \\ \hline u_1 \end{bmatrix} = G_{susn} \begin{bmatrix} X \\ \hline p \\ \hline u_1 \end{bmatrix} \tag{28}$$

The model G_{susn} is a ten-input, eleven-output system as shown in Fig.5 and the above matrices are given in APPENDIX. The input/output relation of G_{susn} can be described by the upper LFT, i.e.,

$$\begin{bmatrix} z_p \\ y \end{bmatrix} = F_u\left(G_{susn}, \Delta_p\right) u_1 \tag{29}$$

with the diagonal parameter uncertain matrix $\Delta_p = \mathrm{diag}\left[\delta_{mb} I_2, \delta_{ks}, \delta_{kt}, \delta_{cf}, \delta_\Phi\right] : \delta_i \in \mathbb{R}, \left|\delta_i\right| \le 1$.

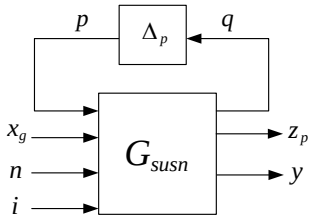

Fig.5 Perturbed suspension model with measurement noises

2.3 Motor Electrical Model

The electrical model of the three-phase permanent-magnet brushless DC motor can be simplified as a classic RL-circuit [21] as depicted in Fig.6.

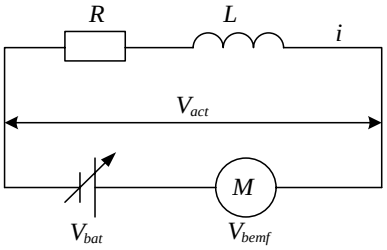

Fig.6 Simplified circuit diagram of DC motor

The back electromotive force V_{bemf} of motor is proportional to the angular velocity as follows:

$$V_{bemf} = K_E \omega = \frac{2\pi K_E}{P_l} v_s \tag{30}$$

in which K_E is voltage constant of motor.

The battery voltage V_{bat} can be adjusted to realize the necessary control current i and the voltage on the equivalent resistance and equivalent inductance V_{act} can be obtained as follows:

$$V_{act} = V_{bat} - V_{bemf} = L\frac{di}{dt} + Ri \tag{31}$$

The nominal transfer function of electrical motor model is considered as a first-order, phase-lag model, i.e.,

$$G_m(s) = \frac{i(s)}{V_{act}(s)} = \frac{1}{Ls + R} = \frac{K_{mc}}{T_{mc}s + 1} \tag{32}$$

where $K_{mc} = 1/R$ and $T_{mc} = L/R$.

Assume that the gain coefficient K_{mc} varies with relative error 10% around its nominal value and the time constant T_{mc} with relative error 20%. In order to account for unmodeled dynamics of motor, the uncertainty is approximated by the input multiplicative uncertainty caused by the perturbed transfer functions as below:

$$G_m(s) = \left(1 + W_m \delta_m\right)\bar{G}_m(s) \tag{33}$$

where $\delta_m \in \mathbb{C}, \left|\delta_m\right| \le 1$ and the uncertainty weighting function W_m is chosen to satisfy the following inequality:

$$\frac{\left|G_m(j\omega) - \bar{G}_m(j\omega)\right|}{\left|\bar{G}_m(j\omega)\right|} < \left|W_m(j\omega)\right| \tag{34}$$

Considering the influence of the variations of K_{mc} and T_{mc}, W_m is obtained as follows:

$$W_m = \frac{0.381s + 36.6466}{s + 359.4713}.$$

Due to writing simplicity, V_{act} is substituted by

u, the block diagram of electrical model with the input multiplicative uncertainty is described by equation (35) as shown in Fig.7.

$$i = F_u(G_{mp}, \delta_m)u \tag{35}$$

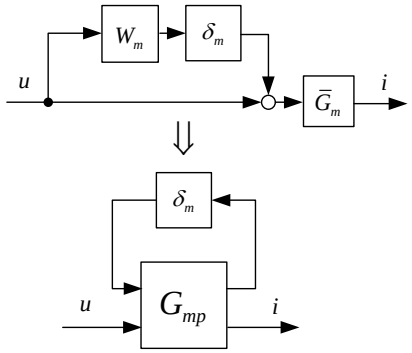

Fig.7 Block diagram of perturbed motor electrical model

2.4 Augmented System Model

Combining suspension model with motor model, the block diagram of entire system can be obtained as shown in Fig.8, in which δ_m is a complex uncertainty and Δ_p are real uncertainties. In order to limit the control voltage within a required range, u is added to the output vector as a performance index. The blocks in the dashed-line frame can be integrated into G_{sys}, and the entire perturbed suspension system can be described by equation (36), as shown in Fig.9,

$$\begin{bmatrix} z \\ y \end{bmatrix} = F_u\left(G_{sys}, \Delta\right)\begin{bmatrix} x_g \\ n \\ u \end{bmatrix} \tag{36}$$

where $z = \begin{bmatrix} z_p & z_u \end{bmatrix}^T$ represents the performance outputs including suspension performances z_p and control input $z_u = u$ and the diagonal uncertainty matrix becomes $\Delta = \mathrm{diag}\left[\Delta_p, \delta_m\right]$.

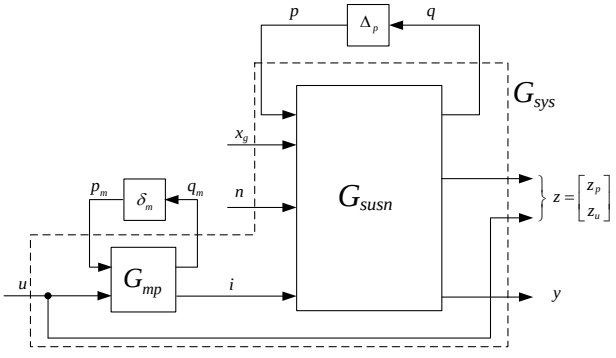

Fig.8 Block diagram of entire system with uncertainties

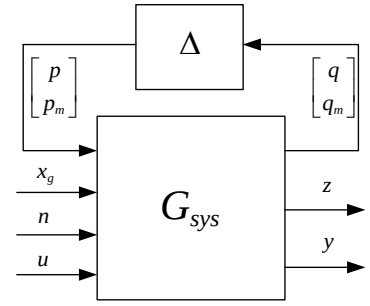

Fig.9 LFT representation of entire system with uncertainties

The closed-loop augmented model, which includes the entire system, the feedback structure, the weighting functions and the controller, as well as the model uncertainties and the performance objectives, is depicted in Fig.10. In the diagram, $\bar{d} = \begin{bmatrix} \bar{w} & \bar{n} \end{bmatrix}^T$ are the inputs of perturbation. The control aim is to reduce ∞ norm of the transfer function matrices from $\bar{d}$ to $\bar{z}$, for all possible uncertainty matrices $\Delta : \|\Delta\|_\infty < 1$. The weighting functions W_i and W_n represent frequency domain models of disturbance $\bar{w}$ and noises $\bar{n}$, respectively, and the weighting functions W_p and W_{uc} are the performance outputs. The dashed-line rectangle represents the augmented model P.

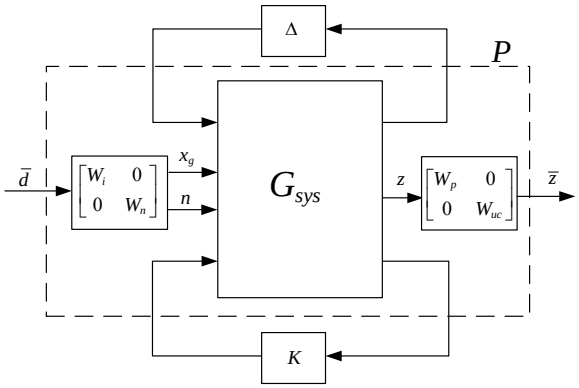

Fig.10 Closed-loop augmented system

3 μ synthesis of augmented system

The closed-loop augmented system in Fig.10 is a standard robust design problem. P and K are interconnected by lower LFT to form a matrix as below:

$$M = F_l\left(P, K\right) = \begin{bmatrix} M_{11} & M_{12} \\ M_{21} & M_{22} \end{bmatrix} \tag{37}$$

with respect to the uncertainty set Δ and a fictitious uncertainty block Δ_f, which is called the performance uncertainty block with $\|\Delta_f\|_\infty \le 1$ as shown in Fig.11.

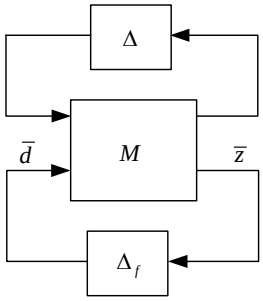

Fig.11 Standard $M-\Delta$ configuration with Δ_f analysis

The nominal performance transfer function can be derived as $\overline{z}=M_{22}\overline{d}$, so the nominal performance requirement can be obtained as:

$$\left\|M_{22}\right\|_\infty<1 \tag{38}$$

Necessary and sufficient conditions for robust stability and robust performance can be formulated in terms of the structured singular value denoted as μ. In order to guarantee the robust stability of the perturbed system, it is required that

$$\mu_\Delta\left(M_{11}(s)\right)<1 \tag{39}$$

in which $\mu_\Delta\left(M_{11}(s)\right):=\sup_{\omega\in\mathbb{R}}\mu_\Delta\left(M_{11}(j\omega)\right)$.

The perturbed performance transfer function can be derived that

$$\overline{z}=\left[M_{22}+M_{21}\Delta\left(I-M_{11}\Delta\right)M_{12}\right]\overline{d}=F_u\left(M,\Delta\right)\overline{d}$$

Thus, the perturbed performance requirement can be set as

$$\left\|F_u\left(M,\Delta\right)\right\|_\infty<1 \tag{40}$$

The inequality (40) is equivalent to the system loop in Fig.11 to be robustly stable with respect to Δ_f . Hence, robust performance can be equivalently considered as a robust stabilization problem with respect to a structured uncertainty $\tilde{\Delta}=\mathrm{diag}\left[\Delta,\Delta_f\right]$, $\left\|\tilde{\Delta}\right\|_\infty\le 1$. The robust performance can be guaranteed by the necessary and sufficient condition as

$$\mu_{\tilde{\Delta}}\left(M(s)\right)<1 \tag{41}$$

where $\mu_{\tilde{\Delta}}\left(M(s)\right):=\sup_{\omega\in\mathbb{R}}\mu_{\tilde{\Delta}}\left(M(j\omega)\right)$.

Based on the above μ analysis, the μ synthesis problem for the augmented model is to find a linear, output controller *K* to generate an output feedback to ensure the inequalities (38), (39) and (41). Or, equivalently, the objective is solve for *K*

$$\sup_{\omega\in\mathbb{R}}\mu_{\tilde{\Delta}}\left[M\left(P,K\right)(j\omega)\right]<1 \tag{42}$$

The *D-K* iteration μ synthesis method [10] is used to solve (42). The method is based on solving the following optimization problem, for a stabilizing controller *K* and a diagonal constant scaling matrix *D*,

$$\inf_K\sup_{\omega\in\mathbb{R}}\inf_{D\in\mathcal{D}}\overline{\sigma}\left[DMD^{-1}(j\omega)\right] \tag{43}$$

where the scaling matrix set $\mathcal{D}$ is defined as

$$\mathcal{D}:\left\{\begin{array}{l}D=\mathrm{diag}\left[D_1,D_2,D_3,D_4,D_5,d_1I_1,I_2\right]:\\ D_1\in\mathbb{C}^{2\times2},D_2\in\mathbb{C}^{1\times1},D_3\in\mathbb{C}^{1\times1},D_4\in\mathbb{C}^{1\times1},\\ D_5\in\mathbb{C}^{1\times1},D_i=D_i^*>0,d_1>0,I_1=I^{1\times1},I_2=I^{3\times4}\end{array}\right\}.$$

Corresponding to inequality (42), the stabilizing controller is to be found such that

$$\sup_{\omega\in\mathbb{R}}\inf_{D\in\mathcal{D}}\overline{\sigma}\left[DMD^{-1}(j\omega)\right]<1 \tag{44}$$

The *D-K* iteration method is to reduce the left-hand-side value of (44), for *K* and *D* in turn while keeping the other one fixed.

The *D-K* iteration algorithm is as follows:

Step 1: start with an initial guess for *D*, usually set *D=I*.

Step 2: fix *D* and solve the H_∞ optimization for *K*, $K=\arg\inf_K\left\|F_l\left(DF_l\left(P,K\right)D^{-1},K\right)\right\|_\infty$.

Step 3: fix *K* and solve the following convex optimization problem for *D* at each frequency over a selected frequency range, $D(j\omega)=\arg\inf_{D\in\mathcal{D}}\overline{\sigma}\left[DF_l\left(P,K\right)D^{-1}(j\omega)\right]$.

Step 4: curve fit $D(j\omega)$ to get a stable , minimum-phase $D(s)$; go to Step 2 and repeat, until inequality (44) is satisfied.

In this study, an H_∞ synthesis controller is also designed concerning the nominal augmented system to compare with the μ synthesis controller. According to the ISO 2631-3, human sensitivity to vibrations is frequency-dependent. The weighting functions are chosen to improve the suspension performances in this frequency range. The weighting functions of both μ synthesis and H_∞ synthesis are determined as follows:

$W_i=0.1$, $W_n=\mathrm{diag}[10^{-3},10^{-3}]$, $W_{uc}=0.0012$, $W_p=\mathrm{diag}[W_{z1},W_{z2},W_{z3}]$

where

$$W_{z1}=5.3\times10^{-5}\frac{s^2+99.4s+14431.9}{s^2+3364.8s+720.9},$$

$$W_{z2}=\frac{s^2+471.6s+7245.1}{s^2+699.2s+1854.3},$$

$$W_{z3}=\frac{2s^2+247.7s+19411.2}{1.1s^2+157.7s+293.8}.$$

4 Simulation results

The simulations for the designed μ synthesis controller and H_∞ synthesis controller have been carried out in MATLAB. The nominal parameters of suspension and motor are chosen based on the practical case for a single real wheel of a small saloon car and shown in Table 1 below. The damping coefficient C_p of passive suspension is $2083\text{N}\cdot\text{s/m}$ and the other parameters of passive suspension are the same as those of active suspension.

Table 1 Nominal parameters of active suspension system

Symbol	Value	Symbol	Value
m_b	255.5	K_T	0.1518
m_w	24.5	K_E	0.1518
K_s	33984	Φ	47.69
K_t	206450	P_l	0.02
C_f	200	R	1.2
J_r	0.15	L	0.004
J_n	0.1	α_1	0.0204
I_d	2.4674	α_2	10

4.1 Frequency responses of the closed-loop nominal model

The frequency responses of the closed-loop nominal suspension model are illustrated in Fig.12. Based on ISO2361 of human response to vibration, the sensitive frequency range, i.e., 4-8 Hz (25-50 rad/s), is chosen to evaluate the designed suspension with both μ and H_∞ synthesis controllers. From Fig.12, it is obvious that BA has been decreased greatly for two active suspensions, which implies that ride comfort can be improved significantly compared with passive suspension. Furthermore, H_∞ synthesis controller achieves slightly less BA than μ synthesis controller in the sensitive frequency range. The price of better ride comfort is that two controllers has a high gain of SWS in the wheel-hop frequency and low frequency under 10 rad/s.

Fig.13 shows the nominal performance of two controllers, which can be quantified by ∞-norm of $\overline{z}/\overline{d}$. It is clear that ∞-norm of the H_∞ synthesis controller is a bit lower, which implies that its nominal performance is a little better than that of the μ synthesis controller. The reason of this conclusion is that the H_∞ synthesis controller is designed for the nominal system without perturbations, while the design of μ synthesis controller takes robust performance of the perturbed system into account, consequently, leading to the cost of nominal performance.

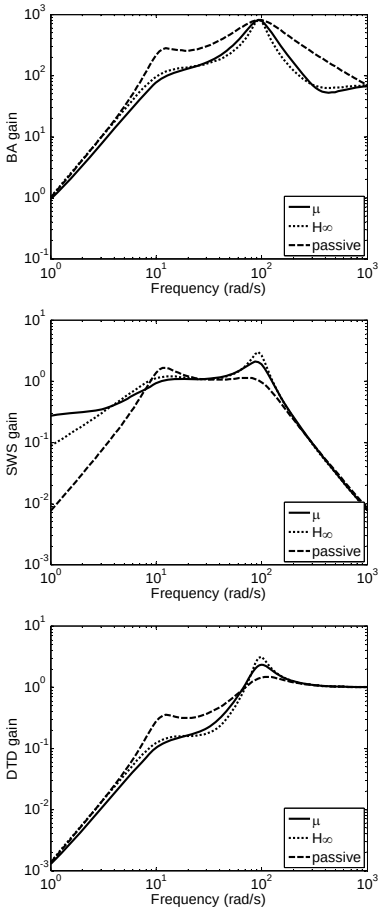

Fig.12 Frequency response of closed-loop nominal model

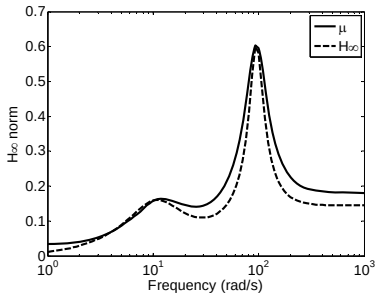

Fig.13 ∞-norm of H_∞ and μ controller

4.2 Time responses of the closed-loop nominal model

In order to test the validity of the designed controllers, a set of simulations in time domain is conducted on random road profile based on the closed-loop nominal model. The road condition is that vehicle is driven on the C-class road whose roughness coefficient is $256\times10^{-6}\,\text{m}^3/\text{cycle}$ at the cruising speed of 20m/s. Fig.14 compares the root-mean-square (RMS) values of suspension performances of both passive and active suspensions.

It can be seen that BA has been reduced 39.81% and 44.46% by μ synthesis controller and H_∞ synthesis controller respectively, compared with passive suspension. Since the random road input is subject to Gaussian distribution, the performance outputs obey a Gaussian distribution for the linear system, which implies that the target RMS values are limited in one third of the maximum values. SWS is designed for the limitation of ± 0.053m, indicating that SWS_{rms} value cannot exceed 0.0177m. Although SWS of active suspension is increased up to 37.5% compared with passive suspension as shown in Fig.14(b), SWS_{rms} is limited still in the required range.

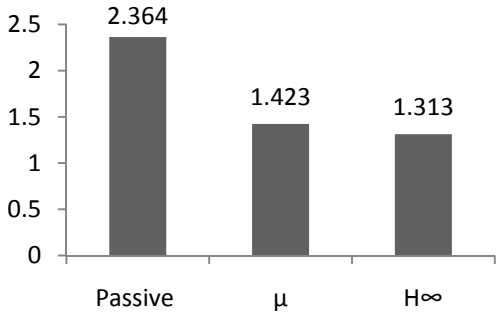

(a) $BA_{rms}(m/s^2)$

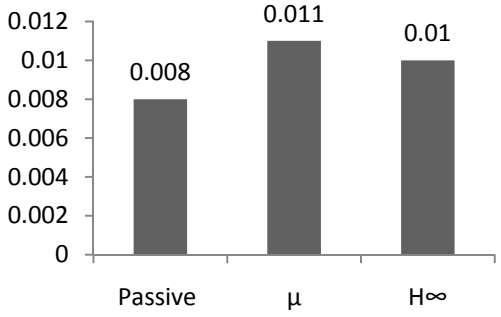

(b) $SWS_{rms}(m)$

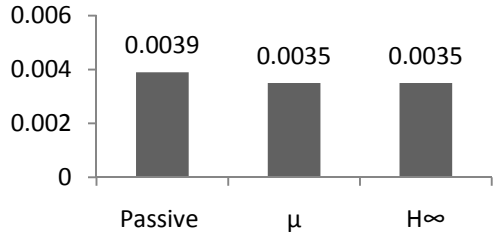

(c) $DTD_{rms}(m)$

Fig.14 RMS values of suspension performances on random road profile

4.3 μ analysis of robust stability and robust performance

Based on inequality (39) and (41), the structured singular value μ of two controllers are calculated to evaluate robust stability and robust performance of the perturbed system. The upper and lower bounds of $\mu_\Delta(M_{11})$ and $\mu_{\tilde{\Delta}}(M)$ with H_∞ synthesis controller are shown in Fig.15. Since the maximum values of $\mu_\Delta(M_{11})$ and $\mu_{\tilde{\Delta}}(M)$ are larger than 1, it can be concluded that robust stability and robust performance of H_∞ synthesis controller cannot be guaranteed.

Fig.16 illustrates the upper and lower bounds of $\mu_\Delta(M_{11})$ and $\mu_{\tilde{\Delta}}(M)$ with μ synthesis controller. The maximum value of $\mu_\Delta(M_{11})$ is only 0.33, indicating that robust stability is achieved, i.e., the system stability is preserved for $\|\Delta\|_\infty < 1/0.33$. The maximum value of $\mu_{\tilde{\Delta}}(M)$ in the robust performance analysis is 0.97, which can ensure the robust performance.

Overall, H_∞ synthesis controller simply focuses on the nominal model, causing the price of robust performance, while μ synthesis controller can meet the requirement of robust performance.

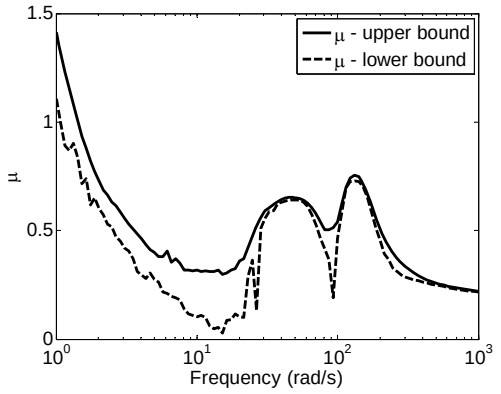

(a) Robust stability

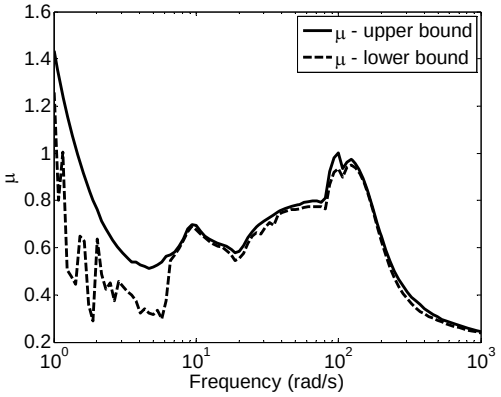

(b) Robust performance

Fig.15 Robust stability and robust performance of H_∞ synthesis controller

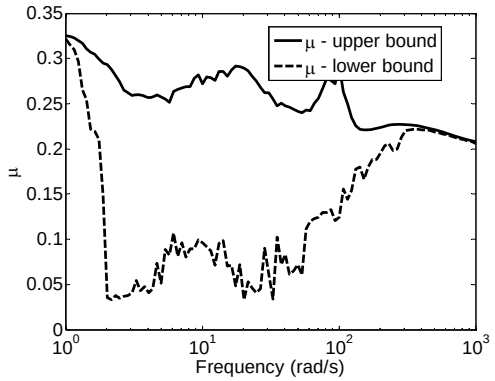

(a) Robust stability

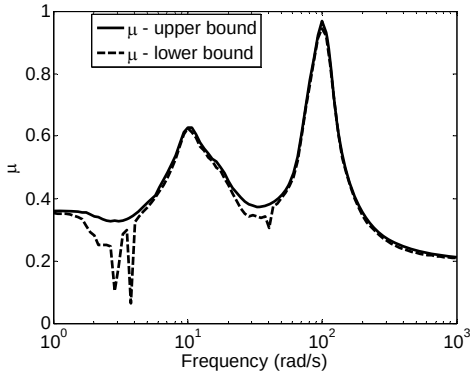

(b) Robust performance

Fig.16 Robust stability and robust performance of μ synthesis controller

4.4 Analysis of sensitive uncertainties

To further illustrate the advantages of μ synthesis controller in robust properties, it is necessary to investigate the effects of five uncertain parameters and unmodeled dynamics on the frequency responses of the perturbed systems. Fig.17 shows the frequency responses of the perturbed systems with m_b variations. Similarly, Fig.18~Fig.22 shows the frequency responses with K_s, K_t, C_f, Φ variations and unmodeled dynamics, respectively. Note that these frequency responses are obtained by assuming that one parameter varies while other variable parameters are frozen.

It can be seen that the curves of frequency responses of BA fluctuate more violently in Fig.17 and Fig.22, which implies that m_b and the unmodeled dynamics are the sensitive factors of ride comfort. Moreover, the curves of SWS in low frequency fluctuate more violently in Fig.21 and Fig.22, indicating that SWS is sensitive to the changes of Φ and the unmodeled dynamics. Hence, it is obvious that m_b, Φ and unmodeled dynamics are the sensitive factors which can influence significantly on the suspension performances. Especially, since the unmodeled dynamics have a direct impact on the active control force, it could be the most important factors in these three sensitive factors.

Additionally, since the curve clusters of the μ synthesis controller are more intensive than those of the H_∞ synthesis controller, it is concluded that the μ synthesis controller has better robustness than the H_∞ synthesis controller, which also verify better robust performance of the μ synthesis controller.

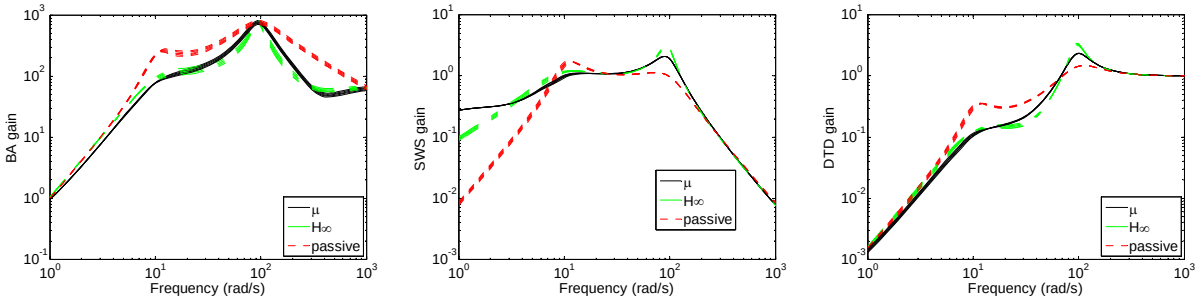

Fig.17 Frequency responses of the perturbed systems with m_b variations

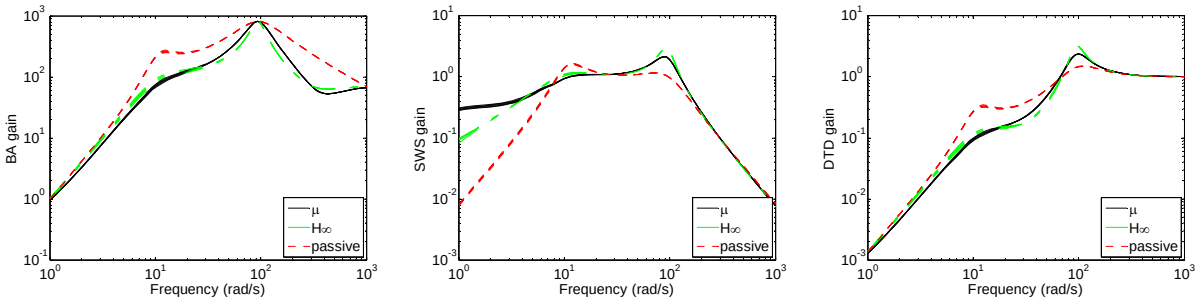

Fig.18 Frequency responses of the perturbed systems with K_s variations

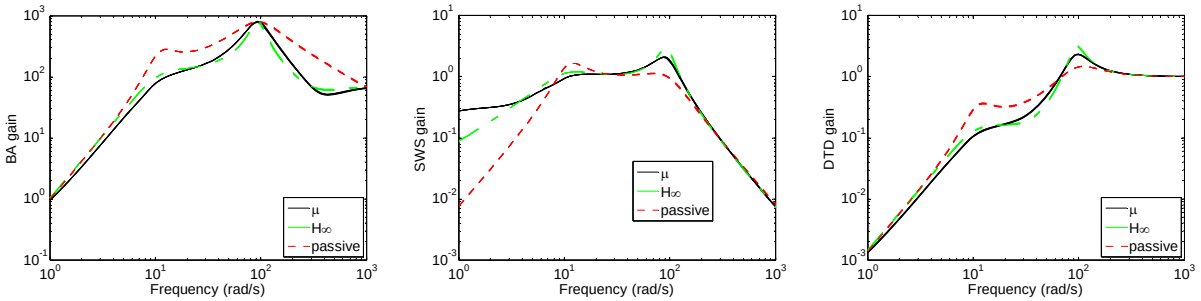

Fig.19 Frequency responses of the perturbed systems with K_t variations

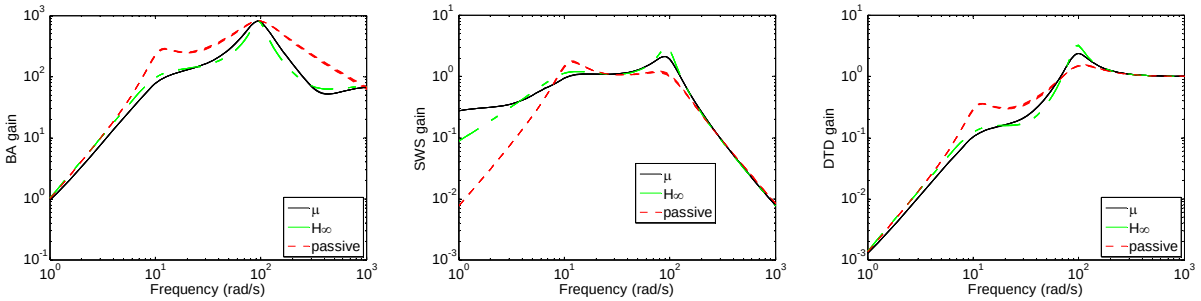

Fig.20 Frequency responses of the perturbed systems with C_f variations

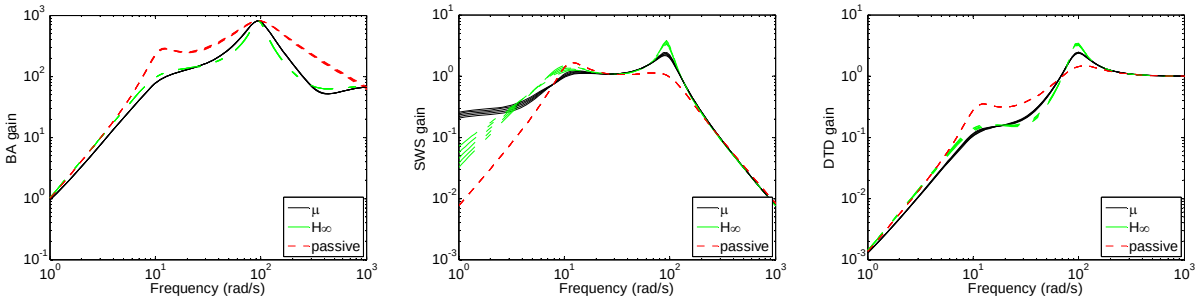

Fig.21 Frequency responses of the perturbed systems with Φ variations

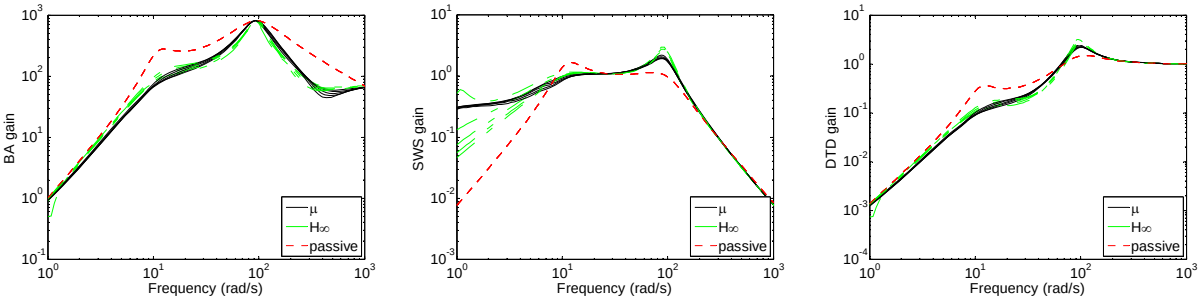

Fig.22 Frequency responses of the perturbed systems with the unmodeled dynamics

5 Conclusions

This paper builds an uncertain model for an active electrical vehicle suspension system taking parameter uncertainties and high-order unmodeled dynamics of suspension and motor actuator into consideration, and then proposes a mixed μ synthesis controller based on *D-K* iteration method to meet the requirement of robust stability and robust performance. In order to examine the feasibility and effectiveness of the proposed controller, simulations are carried out. For comparison purpose, an H_∞ synthesis controller is designed as well. The frequency and time responses show that comparing with passive suspension, the designed μ synthesis controller achieves the significant improvement of ride comfort, while it is slightly worse than the H_∞ synthesis controller in the sensitive frequency range. Furthermore, robust stability and robust performance of the perturbed system are tested by μ analysis. The results indicate that the μ synthesis controller is superior to the H_∞ synthesis controller in robust performance. Finally, the sensitiveness of uncertainties is demonstrated,

showing that m_b, Φ and unmodeled dynamics are sensitive factors compared with K_s, K_t and C_f.

Future research work will be conducted on the performance comparisons between motor actuator and other suspension actuators, e.g., electrohydraulic actuator.

Acknowledgments

This work was supported by National Natural Science Foundation of China (Grant No. 50575141 and No. 50875163). The authors express gratitude to NSFC for the financial support.

References

[1] F. Yu and D. Crolla, State observer design for an adaptive vehicle suspension. *Vehicle System Dynamics*, Vol.30, No.6, 1998, pp. 457-471.

[2] F. Yu, J. Zhang, and D. Crolla, A study of a Kalman filter active vehicle suspension system using correlation of front and rear wheel road inputs. *Proceedings of the Institution of Mechanical Engineers, Part D: Journal of Automobile Engineering*, Vol.214, No.5, 2000, pp. 493-502.

[3] M.M. ElMadany and Z.S. Abduljabbar, Linear quadratic gaussian control of a quarter-car suspension. *Vehicle System Dynamics*, Vol.32, No.6, 1999, pp. 479-497.

[4] M. Yamashita, et al., Application of H∞ control to active suspension systems. *Automatica*, Vol.30, No.11, 1994, pp. 1717-1729.

[5] H. Chen, Z. Liu, and P. Sun, Application of constrained H∞ control to active suspension systems on half-car models. *Journal of Dynamic Systems, Measurement and Control*, Vol.127, 2005, pp. 345-354.

[6] J. Wang, et al., Robust modelling and control of vehicle active suspension with MR damper. *Vehicle System Dynamics*, Vol.46, 2008, pp. 509-520.

[7] A. Stribrsky, K.H.J. Honcu, and A. Kruczek. Active suspension system-experiments. *4th WSEAS/IASME International Conference on DYNAMICAL SYSTEMS and CONTROL*. 2008, Corfu, Greece.

[8] K. Hyniova, et al., Active suspension system with linear electric motor. *WSEAS TRANSACTIONS on SYSTEMS*, Vol.8, No.2, 2009, pp. 278-287.

[9] K. Ales, et al. Automotive active suspension - case study on H-infinity control. *Proceedings of the 13th WSEAS international conference on Automatic control, modelling & simulation*. 2011, Lanzarote, Canary Islands, Spain.

[10] K. Zhou and J.C. Doyle, *Essentials of robust control*. 1998, New Jersey: Prentice Hall.

[11] I. Fialho and G. Balas, Road adaptive active suspension design using linear parameter-varying gain-scheduling. *IEEE transactions on control systems technology*, Vol.10, No.1, 2002, pp. 43-54.

[12] P. Gaspar, I. Szaszi, and J. Bokor, Active suspension design using linear parameter varying control. *International Journal of Vehicle Autonomous Systems*, Vol.1, No.2, 2003, pp. 206-221.

[13] A. Zin, et al. An LPV/H∞ active suspension control for global chassis technology: design and performance analysis. *American Control Conference*. 2006.

[14] A. Zin, et al., Robust LPV/H∞ control for active suspensions with performance adaptation in view of global chassis control. *Vehicle System Dynamics: International Journal of Vehicle Mechanics and Mobility*, Vol.46, No.10, 2008, pp. 889 - 912.

[15] P. Gaspar, et al. Active suspension design based on mixed uncertainty modeling. *European Control Conference*. 2001, Porto, Portugal.

[16] P. Gaspar, I. Szaszi, and J. Bokor, Design of robust controllers for active vehicle suspension using the mixed μ synthesis. *Vehicle System Dynamics*, Vol.40, No.4, 2003, pp. 193-228.

[17] F. Yu and X.C. Zheng. Study on the potential benefits of an energy-regenerative active suspension for vehicles. *SAE paper*. 2005-01-3564.

[18] X. Zheng, F. Yu, and Y. Zhang, A novel energy-regenerative active suspension for vehicles. *Journal of Shanghai Jiaotong University (Science)*, Vol.13, No.2, 2008, pp. 184-188.

[19] Y. Zhang, F. Yu, and K. Huang. Permanent-magnet DC motor actuators application in automotive energy-regenerative active suspensions. *SAE paper*. 2009-01-0227.

[20] D. Hrovat, Survey of advanced suspension developments and related optimal control applications. *Automatica*, Vol.33, No.10, 1997, pp. 1781-1817.

[21] K. Huang, Y. Zhang, and F. Yu, Predictive controller design for electromagnetic suspension based on mixed logical dynamical model. *Journal of Vibration and Control*, Vol., 2011.

Appendix
Notation

Symbol	Description	Symbol	Description
BA	Body acceleration, m/s^2	m_w	Wheel mass, kg
C_f	Equivalent damping coefficient, $N\cdot s/m$	P_l	Lead of ball screw, m
C_p	Passive damping coefficient, $N\cdot s/m$	R	Resistance, Ω
DTD	Dynamic tire displacement, m	SWS	Suspension working space, m
i	Motor current, A	T_m	Motor output torque, $N\cdot m$
I_d	Equivalent inertia, kg	T_{mc}	Time constant of motor
J_n	Moment of inertia of nut, $kg\cdot cm^2$	T_o	Actual total output torque, $N\cdot m$
J_r	Moment of inertia of rotor, $kg\cdot cm^2$	V_{bemf}	Back electromotive force, V
K_E	Voltage constant of motor, $V\cdot s/rad$	V_{bat}	Battery voltage, V
K_{mc}	Gain coefficient of motor	Φ	Motor constant, N/A
K_s	Suspension stiffness, N/m	α_1	Gain of accelerometer, $V\cdot s^2/m$
K_t	Tire stiffness, N/m	α_2	Gain of displacement meter, V/m
K_T	Torque constant of motor, $N\cdot m/A$	θ	Rotation angle, rad
L	Inductance, H	ω	Angular velocity, rad/s
m_b	Body mass, kg		

$$A=\begin{bmatrix} 0 & 1 & 0 & 0 \\ -\beta m_w\bar{K}_s & -\beta m_w\bar{C}_f & \beta\left(m_w\bar{K}_s-I_d\bar{K}_t\right) & \beta m_w\bar{C}_f \\ 0 & 0 & 0 & 1 \\ \gamma_1\left(1-\beta\gamma_2\right)\bar{K}_s & \gamma_1\left(1-\beta\gamma_2\right)\bar{C}_f & \gamma_1\left(\beta\gamma_2-1\right)\left(\bar{K}_s+\bar{K}_t\right)-\beta I_d\bar{K}_t & \gamma_1\left(\beta\gamma_2-1\right)\bar{C}_f \end{bmatrix}$$

$$B_p=\begin{bmatrix} 0 & 0 & 0 & 0 & 0 & 0 \\ -\alpha & 0 & -\beta m_w d_{ks} & -\beta I_d d_{kt} & -\beta m_w d_{cf} & \beta m_w d_\Phi \\ 0 & 0 & 0 & 0 & 0 & 0 \\ 0 & -\alpha & \gamma_1\left(1-\beta\gamma_2\right)d_{ks} & \left(-\gamma_1+\beta\gamma_1\gamma_2-\beta I_d\right)d_{kt} & \gamma_1\left(1-\beta\gamma_2\right)d_{cf} & \gamma_1\left(\beta\gamma_2-1\right)d_\Phi \end{bmatrix}$$

$$B_1=\begin{bmatrix} 0 & 0 & 0 \\ \beta I_d\bar{K}_t & 0 & 0 \\ 0 & 0 & 0 \\ \left(\gamma_1-\beta\gamma_1\gamma_2+\beta I_d\right)\bar{K}_t & 0 & 0 \end{bmatrix},\ B_2=\begin{bmatrix} 0 \\ \beta m_w\bar{\Phi} \\ 0 \\ \gamma_1\left(\beta\gamma_2-1\right)\bar{\Phi} \end{bmatrix}$$

$$C_q=\begin{bmatrix} -\beta m_w\bar{K}_s & -\beta m_w\bar{C}_f & \beta\left(m_w\bar{K}_s-I_d\bar{K}_t\right) & \beta m_w\bar{C}_f \\ -\beta\gamma_1\gamma_2\bar{K}_s & -\beta\gamma_1\gamma_2\bar{C}_f & \beta\gamma_1\gamma_2\left(\bar{K}_s+\bar{K}_t\right)-\beta I_d\bar{K}_t & \beta\gamma_1\gamma_2\bar{C}_f \\ \bar{K}_s & 0 & -\bar{K}_s & 0 \\ 0 & 0 & \bar{K}_t & 0 \\ 0 & \bar{C}_f & 0 & -\bar{C}_f \\ 0 & 0 & 0 & 0 \end{bmatrix}$$

$$C_z=\begin{bmatrix} -\beta m_w\bar{K}_s & -\beta m_w\bar{C}_f & \beta\left(m_w\bar{K}_s-I_d\bar{K}_t\right) & \beta m_w\bar{C}_f \\ 1 & 0 & -1 & 0 \\ 0 & 0 & 1 & 0 \end{bmatrix}$$

$$C_y=\begin{bmatrix} -\alpha_1\beta m_w\bar{K}_s & -\alpha_1\beta m_w\bar{C}_f & \alpha_1\beta\left(m_w\bar{K}_s-I_d\bar{K}_t\right) & \alpha_1\beta m_w\bar{C}_f \\ \alpha_2 & 0 & -\alpha_2 & 0 \end{bmatrix}$$

$$D_{qp}=\begin{bmatrix} -\alpha & 0 & -\beta m_w d_{ks} & -\beta I_d d_{kt} & -\beta m_w d_{cf} & \beta m_w d_\Phi \\ 0 & -\alpha & -\beta\gamma_1\gamma_2 d_{ks} & \beta\left(\gamma_1\gamma_2-I_d\right)d_{kt} & -\beta\gamma_1\gamma_2 d_{cf} & \beta\gamma_1\gamma_2 d_\Phi \\ 0 & 0 & 0 & 0 & 0 & 0 \\ 0 & 0 & 0 & 0 & 0 & 0 \\ 0 & 0 & 0 & 0 & 0 & 0 \\ 0 & 0 & 0 & 0 & 0 & 0 \end{bmatrix}, \quad D_{q1}=\begin{bmatrix} \beta I_d\bar{K}_t & 0 & 0 \\ \beta\left(I_d-\gamma_1\gamma_2\right)\bar{K}_t & 0 & 0 \\ 0 & 0 & 0 \\ -\bar{K}_t & 0 & 0 \\ 0 & 0 & 0 \\ 0 & 0 & 0 \end{bmatrix},$$

$$D_{q2}=\begin{bmatrix} \beta m_w\bar{\Phi} \\ \beta\gamma_1\gamma_2\bar{\Phi} \\ 0 \\ 0 \\ 0 \\ \bar{\Phi} \end{bmatrix}, D_{zp}=\begin{bmatrix} -\alpha & 0 & -\beta m_w d_{ks} & -\beta I_d d_{kt} & -\beta m_w d_{cf} & \beta m_w d_\Phi \\ 0 & 0 & 0 & 0 & 0 & 0 \\ 0 & 0 & 0 & 0 & 0 & 0 \end{bmatrix}$$

$$D_{yp}=\begin{bmatrix} -\alpha_1\alpha & 0 & -\alpha_1\beta m_w d_{ks} & -\alpha_1\beta I_d d_{kt} & -\alpha_1\beta m_w d_{cf} & \alpha_1\beta m_w d_\Phi \\ 0 & 0 & 0 & 0 & 0 & 0 \end{bmatrix}$$

$$D_{z1}=\begin{bmatrix} \beta I_d\bar{K}_t & 0 & 0 \\ 0 & 0 & 0 \\ -1 & 0 & 0 \end{bmatrix}, D_{z2}=\begin{bmatrix} \beta m_w\bar{\Phi} \\ 0 \\ 0 \end{bmatrix}, D_{y1}=\begin{bmatrix} \alpha_1\beta I_d\bar{K}_t & 1 & 0 \\ 0 & 0 & 1 \end{bmatrix}, D_{y2}=\begin{bmatrix} \alpha_1\beta m_w\bar{\Phi} \\ 0 \end{bmatrix}$$